



HAL
open science

White-matter degradation and dynamical compensation support age-related functional alterations in human brain

Spase Petkoski, Petra Ritter, Viktor K Jirsa

► **To cite this version:**

Spase Petkoski, Petra Ritter, Viktor K Jirsa. White-matter degradation and dynamical compensation support age-related functional alterations in human brain. *Cerebral Cortex*, 2023, 33 (10), pp.6241 - 6256. 10.1093/cercor/bhac500 . hal-04134843

HAL Id: hal-04134843

<https://amu.hal.science/hal-04134843>

Submitted on 20 Jun 2023

HAL is a multi-disciplinary open access archive for the deposit and dissemination of scientific research documents, whether they are published or not. The documents may come from teaching and research institutions in France or abroad, or from public or private research centers.

L'archive ouverte pluridisciplinaire **HAL**, est destinée au dépôt et à la diffusion de documents scientifiques de niveau recherche, publiés ou non, émanant des établissements d'enseignement et de recherche français ou étrangers, des laboratoires publics ou privés.



Distributed under a Creative Commons Attribution - NonCommercial 4.0 International License

White-matter degradation and dynamical compensation support age-related functional alterations in human brain

Spase Petkoski^{1,*}, Petra Ritter^{2,3,4}, Viktor K. Jirsa¹

¹Aix Marseille Univ, INSERM, INS, Inst Neurosci Syst, Marseille, France,

²Berlin Institute of Health at Charité - Universitätsmedizin Berlin, Berlin, Germany,

³Department of Neurology with Experimental Neurology, Brain Simulation Section, Charité - Universitätsmedizin Berlin, Corporate Member of Freie Universität Berlin and Humboldt-Universität zu Berlin, Berlin, Germany,

⁴Bernstein Focus State Dependencies of Learning, Bernstein Center for Computational Neuroscience, Berlin, Germany

*Corresponding author: Institut de Neurosciences des Systèmes UMR INSERM 1106, Aix-Marseille Université Faculté de Médecine, 27, boulevard Jean Moulin, 13005 Marseille, France. Email: spase.petkoski@univ-amu.fr

Structural connectivity of the brain at different ages is analyzed using diffusion-weighted magnetic resonance imaging (MRI) data. The largest decrease of streamlines is found in frontal regions and for long inter-hemispheric links. The average length of the tracts also decreases, but the clustering is unaffected. From functional MRI we identify age-related changes of dynamic functional connectivity (dFC) and spatial covariation features of functional connectivity (FC) links captured by metaconnectivity. They indicate more stable dFC, but wider range and variance of MC, whereas static features of FC did not show any significant differences with age. We implement individual connectivity in whole-brain models and test several hypotheses for the mechanisms of operation among underlying neural system. We demonstrate that age-related functional fingerprints are only supported if the model accounts for: (i) compensation of the individual brains for the overall loss of structural connectivity and (ii) decrease of propagation velocity due to the loss of myelination. We also show that with these 2 conditions, it is sufficient to decompose the time-delays as bimodal distribution that only distinguishes between intra- and inter-hemispheric delays, and that the same working point also captures the static FC the best, and produces the largest variability at slow time-scales.

Key words: brain aging; connectome; dynamic functional connectivity; brain network model; compensation.

Introduction

Combining network dynamics approaches with graph theory metrics is a leading paradigm for studying the brain. The former is motivated by the observations that the brain architecture shapes its neurophysiological activity (Sporns et al. 2004; Vincent et al. 2007; Wang et al. 2013). As a consequence, in the study of its large-scale dynamics, the brain is typically represented as a network of anatomically interacting regions each constrained by inherent dynamics Sanz-Leon et al. (2015); Pathak et al. (2022a). Based on this, a number of modeling studies have demonstrated that independently of the size of the regions and their underlying dynamics, neuroanatomical constraints of the human brain shape and drive its functionality during healthy resting state (Courtiol et al. 2020; Deco et al. 2009; 2011; Schirner et al. 2018) or during pathologies such as epilepsy (Jirsa et al. 2017), stroke (Allegra Mascaro et al. 2020), and Alzheimer's disease (Stefanovski et al. 2019).

Development of the network neuroscience (Bassett and Sporns, 2017) has been possible due to advances of non-invasive structural (Johansen-Berg and Rushworth, 2009) and functional (Logothetis et al. 2001) brain imaging. The former allows drawing a comprehensive map of biologically realistic connectivity, the so-called connectome (Sporns et al. 2005). On the functional side, until recently the focus of research was on the functional

connectivity (FC) that calculates co-fluctuations in the blood oxygenation-level dependent (BOLD) functional magnetic resonance imaging (fMRI) of distant brain regions (Friston, 2011). It is now established that non-stationarity in FC reveals a rich structure characterized by rapid transitions between few discrete FC states, which is captured by the so-called dynamic functional connectivity (dFC) (Hansen et al. 2015; Hutchison et al. 2013).

Aging of the brain is well described, both structurally and functionally. It leads to a substantial overall decrease in the number of streamlines (Bethlehem et al. 2022; Lim et al. 2015; Perry et al. 2015; Peters and Sethares, 2006), which mostly affects inter-hemispheric links that decrease with advancing age (Duffy et al. 1996; Kikuchi et al. 2000; Knott and Harr, 1997). On the functional side, applying graph theory metrics reveals age-related increases of between- and decreases of within-network resting-state FC (Stumme et al. 2020). Temporal variations of the occupancy of FC states during rest are more predictive in the context of aging (Chen et al. 2017). Related to this is the stability of the different states (Li et al. 2020), which has predictive value across lifespan (Sastry et al. 2022), where the total transition of states is negatively correlated with age (Xia et al. 2019). Slowing down with age for dFC is also seen when it is characterized as a random walk

Received: June 20, 2022. Revised: November 2, 2022. Accepted: November 3, 2022

© The Author(s) 2023. Published by Oxford University Press. All rights reserved. For permissions, please e-mail: journals.permission@oup.com

This is an Open Access article distributed under the terms of the Creative Commons Attribution Non-Commercial License (<https://creativecommons.org/licenses/by-nc/4.0/>), which permits non-commercial re-use, distribution, and reproduction in any medium, provided the original work is properly cited. For commercial re-use, please contact journals.permissions@oup.com

(Battaglia et al. 2020), whereas its modular slowing is associated with cognitive dysfunction (Lombardo et al. 2020).

The observed patterns between the structure and the function have been statistically linked (Betz et al. 2014; Zimmermann et al. 2016), but the dependence still has not been established on individual level. A possible link was shown between the decrease of complexity of brain's function in aging and its structural changes represented as long-range pruning (Nakagawa et al. 2013). Variability in neural systems has been associated with functional benefits (Garrett et al. 2011; Sleimen-Malkoun et al. 2014), and its loss with aging is often followed with compensatory and adaptive processes (Lövdén et al. 2010), as well as, dedifferentiation (Baltes and Lindenberger, 1997). However, these have not been linked to the structural loss, which is consistently shown not to have a significant role in age-related cognitive decline (Burke and Barnes, 2006).

Most studies show greatest structural deficit in the frontal regions of the brain and there are regional differences in white matter hyperintensities (Peters, 2006), which most likely result from demyelination and reduce axons' transmission speed (Wen and Sachdev, 2004). Specifically, there is strong evidence that age and loss of myelin integrity reduce conduction velocity along nerve fibers (Peters, 2002). One of the possible mechanisms are myelin sheath alterations, which are strongly correlated with aging in monkeys (Peters and Sethares 2002). As for the direct evidence of conduction velocity reduction, in cats for example has been found that along nerve fibers in the pyramidal tracts it is decreased by 43% for old cats compared to young ones (Xi et al. 1999).

The work that we present has three main goals: (i) to characterize the spatial distribution of the decrease in structural connectivity including the lengths of white matter tracts; (ii) to identify the changes in dynamics of the FC and its higher order spatial features, and (iii) to apply a mechanistic model to test under which conditions the individual structural connectivity can be responsible for (ii). The workflow is illustrated in Fig. 1. The model allows expressing several hypotheses for the impact of demyelination on the propagation velocity (no impact or decrease by 30% and 50%) and for the existence of dynamical compensation for the lost connectivity. For the analysis of structural connectivity, of particular interest are the time delays due to signal transmission (estimated from the ratio tract length and propagation velocity), which determine the synchronization of oscillatory processes (Petkoski et al. 2018; Petkoski and Jirsa, 2019). Time delays and the weights compose the space-time structure of the connectivity that is crucial in shaping its macroscopic activity (Deco et al. 2009; Ghosh et al. 2008; Sanz-Leon et al. 2015). Their impact during synchronization can be unified in the so-called normalization of the connectome for communication through coherence (Petkoski and Jirsa, 2022) that allows graph theoretical metrics to unveil structural affinity for spectrally dependent activation patterns in the brain. Functional alterations are studied through statistics on dFC and MC, which capture temporal and spatial aspects of the FC (Arbasyazd et al. 2020). In particular, for the former we analyze the rate at which transitions occur between overall FC states, and for the latter we analyze the coherence between the pairs of brain regions. For the last part of the study, we utilize Kuramoto oscillators, which despite being overly simple, due to their parsimonious parametrization allow for drawing specific links between network structure and the emergent synchronization patterns of neuronal activity (Allegra Mascaro et al. 2020; Cabral et al. 2011; Pope et al. 2021).

Materials and methods

Data acquisition

In this study we analyze anatomical and diffusion-weighted images of 50 subjects acquired at Berlin Center for Advanced Imaging, Charité University Medicine, Berlin, Germany (age ranged from 18 to 80 years, mean 41.26 ± 18.36 ; 30 females and 20 males). A total of 49 of these subjects were used in the study for describing the automated pipeline for constructing individualized virtual brains from multimodal neuroimaging data (Schirner et al. 2015) and their dFC were also analyzed as part of a larger cohort (Battaglia et al. 2020). The pipeline combines several state-of-the-art neuroinformatics tools to generate subject-specific cortical and subcortical parcellations, surface-tessellations, structural and functional connectomes, lead field matrices, electrical source activity estimates and region-wise aggregated BOLD fMRI time-series (Schirner et al. 2015).

Construction of Structural Connectivity (SC) networks

Desikan–Killiany atlas (Desikan et al. 2006) is used as implemented in FREESURFER (excluding the corpus callosum, but including the insular cortices of both hemispheres) leading to 68 cortical regions of interest (ROI). Details about the magnetic resonance imaging (MRI) acquisition are given in [Supplementary Material 6.2](#). fMRI data were pre-processed following Schirner et al. (2015) and in a same manner as in Battaglia et al. (2020), (details described in [Supplementary Material 6.3](#)).

Upon tractography, the pipeline (Schirner et al. 2015) (see details in [Supplementary Material 6.1](#)) computes distinct connections and aggregates them for each region to generate 3 types of SC matrices:

- raw counts, contain counts of all tracts that were found between each pair of regions (symmetric),
- distinct connection counts, contain only distinct connections between each pair of regions (symmetric),
- weighted distinct connection counts, in which the strength of each distinct connection is divided by the number of all distinct connections leaving the voxel (yielding asymmetric strength matrices).

For the last case, a symmetric SC matrix was constructed by taking the mean of the weights per each direction of the links.

Along with strengths, the pipeline outputs three different SC distances matrices that contain the mean, mode, and median lengths of all tracks that were found between each pair of regions. The means are chosen to represent the distance of the links between each pair of brain regions. Since the actual white matter fibers do not necessarily follow straight lines, these are by construction larger than the Euclidean distances between the ROIs, and also than the distances between the centers of the brain regions.

Modularity

The optimal community structure of the connectomes was calculated using the Louvain function (Blondel et al. 2008) from the Brain Connectivity Toolbox (Rubinov and Sporns, 2010) for weighted undirected links. The algorithm was run starting from a value of the resolution parameter, which gives twice the number of the required partitions. Then the resolution parameter was decreased by 1% at each consecutive step until a partition consisting of a predefined number of communities was achieved. The procedure was repeated 100 times each, for partitions of

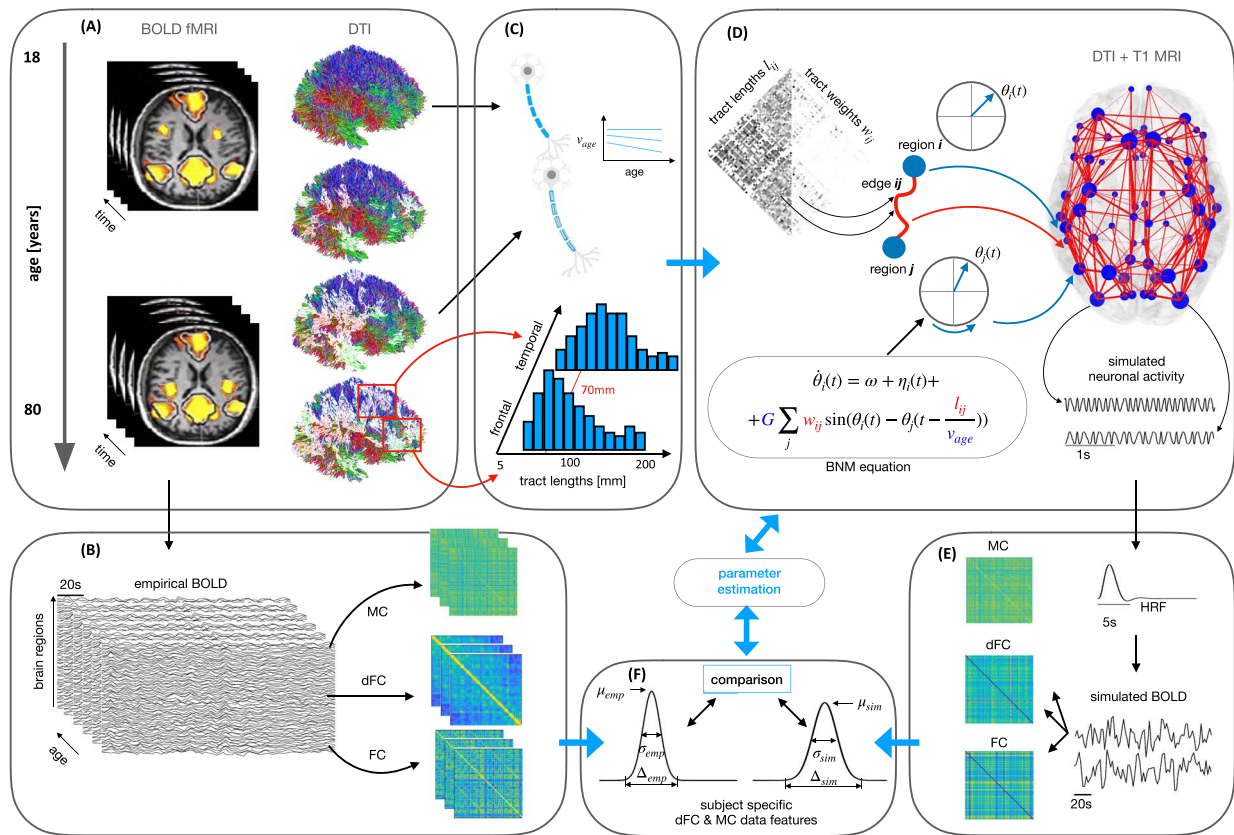


Fig. 1. Data analysis and modeling workflow. A) fMRI and DTI are performed in a cohort in the age range from 18 to 80 years. B) Static, dynamic, and spatial higher order connectivity are calculated for the empirical BOLD fMRI time-series of each subject. C) Structural connectivity (SC) is reconstructed from DTI and is characterized with the respect of number and length of the tracts, as well as their location in the brain (lobes and hemispheres). The impact of the aging-induced demyelination is linearly accounted in axonal velocity, from which time delays are assigned to each link, based on its length and subject's age. D) Together with the weights for the coupling between brain nodes, time-delays build the brain network model of Kuramoto oscillators. These are subject specific (shown in red in the model equation) and fixed, whereas the global coupling G and the age-dependent mean axonal propagation velocity v_{age} are the only free hyper-parameter. E) Simulated neuronal activity is passed through a hemodynamic response function to yield BOLD time-series. The same procedures as for the empirical data are used to calculate FC, dFC, and MC for the static, dynamic, and spatial higher order connectivity of the simulated data. F) Different data features are extracted for each of the connectivity metrics, and they are compared for the empirical and simulated data. By parameters sweep we estimate the parameters of the model that best fit the data.

2, 3, 4, and 5 communities. For each of these repetitions and partitions, we calculated the modularity coefficient Q , which is a scalar between -1 and 1 that measures the density of links inside communities as compared with links between communities (Newman and Girvan, 2004). In addition we calculated the modularity coefficient for the initial community affiliation set to correspond exactly to the left and right hemispheres. Here again an algorithm was run for the same 100 resolution parameters that earlier achieved optimal bi-community structure, until it was assured that the division in 2 communities corresponds to the hemispheric division.

dFC metrics

Static (time-averaged) FC is calculated as Pearson correlation of the BOLD time-series, empirical or simulated, in a given time window. This is a linear metric that describes statistical dependencies, in a similar sense as coherence, or transfer entropy (Friston, 2011). Other possibility would be to focus on metrics of information flow and complexity such as spectral Granger causality (Faes et al. 2017) and multiscale entropy (Costa et al. 2002), which in addition account for nonlinear and multi-scale interactions of brain signals (Courtiol et al. 2016).

Evolution of FC over time is captured by dFC that is defined the same as functional connectivity dynamics (FCD) in

Hansen et al. (2015). It describes the similarity between $FC(t)$ matrices at different time windows t_k , where $k = 1 \dots M$. The (t_k, t_l) entry of the $M \times M$ FCD matrix is provided by the Pearson correlation between the upper triangular parts of the 2 matrices $FC(t_k)$ and $FC(t_l)$ (Arbasyazd et al. 2020). We calculated FCD for 4 different window sizes (30, 15, 10, and 5 time points), which always move by 1 time point. In all the cases, by keeping the interval between two consecutive FC network time-resolved estimations constant, higher and lower correlations of the FCD can naturally be interpreted as associated to a slower or faster speed of dFC reconfiguration (Battaglia et al. 2020). Hence, a first aim to describe dFC consists of a suitable quantification and description of the distributions of FCD entries, notably, their mean, median or mode, giving a typical dFC speed, and their spread as given by their second and higher momenta, i.e. standard deviation (STD) and kurtosis.

In addition we calculated higher order interactions between brain regions using metaconnectivity (MC) (Arbasyazd et al. 2020). Exactly as typical static FC analysis ignores time, the previously mentioned FCD analyses ignore space. However, FC reconfiguration may occur at different speeds for different sets of links (Lombardo et al. 2020). Furthermore, the fluctuations of certain FC links may coincide with the fluctuation of other FC links, but at the same time be relatively independent from the fluctuation

of other sets of links. Therefore, we compute a different dFC speed distribution for different sets of links, which constitute spatial dFC modules. MC is defined as correlation between linkwise time-series consisting of the pairwise correlations between the given nodes at each window. Hence it represents a fourth order statistics between nodes' dynamics. Links in the MC matrices are grouped in a such a way that besides the overall MC, we also calculate the statistics of the links within the left and within the right hemispheres, between the hemispheres, between the internal left versus right hemispheric links, and left and right versus inter-hemispheric each. These are all illustrated in Fig. 4, where the MC within the 7 clusters is expected to be distinctive, as a consequence of the high hemispheric bimodularity of the SC discussed in Section 2.3

Model

Brain Network Model (BNM) with Kuramoto oscillators

Personalized BNM comprises 68 delay-coupled cortical brain regions, each having a dynamics captured by Kuramoto oscillators (Cabral et al. 2011; Petkoski et al. 2018; Pope et al. 2021). Weighted distinct connection counts are chosen as connectivity strengths, because they account for most physiological features (Schirmer et al. 2016; 2018). Time delays of each link are defined from the individual lengths by setting the propagation velocity at 3.3m/s, which was shown to have a highest predictive value for supporting realistic spectral activation patterns (Petkoski and Jirsa, 2022) and is a value between the empirical mean and median cortico-cortical evoked potentials (Lemaréchal et al. 2021). To confirm the generality of the results, we also use propagation velocities of 2m/s and 5m/s.

We consider the Kuramoto model (KM) (Kuramoto, 1984) with explicit heterogeneous time-delays τ_{ij} and coupling strengths Gw_{ij} , where G is a global coupling parameter and w_{ij} are the normalized weights from the connectome. This represents a canonical model for weakly, delay-coupled oscillators, with long delays in comparison to the coupling strengths or natural frequencies (Ermentrout and Wechselberger, 2009). For symmetric, link-dependent delays, $\tau_{ij} = \tau_{ji}$, and phases θ_i of each oscillator evolve as

$$\dot{\theta}_i = \omega + \frac{G}{N} \sum_{j=1}^N w_{ij} \sin[\theta_j(t - \tau_{ij}) - \theta_i] + \xi_i(t), \quad i = 1 \dots N, \quad (1)$$

where $\omega = 2\pi f$ is the natural frequency of the oscillators. $\xi_i(t)$ takes into account the contribution of different stochastic forces and are assumed to be sources of Gaussian white noise satisfying $\langle \xi_i(t) \rangle = 0$, $\langle \xi_i(t)\xi_j(t') \rangle = 2D\delta_{ij}\delta(t - t')$.

The heterogeneity in phase models can stem from natural frequencies and/or from additive noise term, but both sources have similar influence to the observed global dynamics (Acebrón et al. 2005). The size of the connectome-derived networks is rather small, $N = 68$ cortical regions, and the connection strengths span almost across 5 orders of magnitude. Hence if the natural frequencies were heterogeneous, then the global dynamics would have been highly influenced by the particular realization of the probability density function of the natural frequencies (Petkoski et al. 2018). To avoid this, we fix the natural frequencies of each node, while still introducing heterogeneity to each oscillator in the form of independent white noises with the same intensity.

For the parameters space, we explore only the global coupling G and the propagation velocity v , while keeping fixed the noise D and the frequencies f . This is justified because the dynamics for the KM in general depends on the ratio G/D (Acebrón et al. 2005).

Similarly the impact of the time-delays depend on their relative size compared to the natural frequencies (Petkoski et al. 2016).

BNM with reduced distribution of delays

The reduced model is derived from the decomposition of the space-time structure of the connectome (Petkoski et al. 2016; 2018). It assumes bimodal δ -distributed time-delays, with values corresponding to the mean delays of the internal and external links for each subject. The model hence read

$$\begin{aligned} \dot{\theta}_i &= \omega + \xi_i(t) \\ &+ \frac{G}{N} \sum_{j=1}^{N/2} \begin{cases} w_{ij} \sin[\theta_j(t - \tau_{int}) - \theta_i] + w_{i,j+N/2} \sin[\theta_{j+N/2}(t - \tau_{ext}) - \theta_i], & i = 1 \dots \frac{N}{2} \\ w_{i,j+N/2} \sin[\theta_{j+N/2}(t - \tau_{int}) - \theta_i] + w_{ij} \sin[\theta_j(t - \tau_{ext}) - \theta_i], & i = 1 + \frac{N}{2} \dots N. \end{cases} \end{aligned} \quad (2)$$

Simulated BOLD

Simulated neural activity was converted into simulated BOLD signals using Balloon–Windkessel model (Friston et al. 2003) of The Virtual Brain (Sanz-Leon et al. 2015) and the resulting time-series were then downsampled at 2s, to correspond to the empirical BOLD signals. The physical quantity whose variations underlie BOLD signal was chosen as $b_i = \sin \theta_i$, as it has been the case in other studies of the neuronal activity using Kuramoto oscillators (Cabral et al. 2011; Pope et al. 2021).

Results

White matter loss

Global changes in the SC

A known feature of the connectome of the aging brain is the decrease of total number of connections. Results in Fig. 2 (top) show that this is robustly reflected in all three metrics for the weights: raw counts, distinct connection counts, and weighted distinct connection counts (Schirmer et al. 2015). Mostly affected are the weighted distinct connection counts, which are taking into account the surface of the gray-white matter interface, while avoiding multiple counting of different tracks, and as such are mostly used as connection weights (Schirmer et al. 2018).

Spatial changes in the SC

Next, we investigated if the drop in the number of connections is spatially uniform and to what extent it is affecting the links of different lengths. We analyzed the changes of the intra- and inter-hemispheric links, and of the long and short connections, where the boundary is set at 70mm, so that it corresponds to the local minimum in the global distribution, Fig. S1. These results imply that the loss of connection strength is spatially and across lengths heterogeneous, with long and external links the strongest affected, Fig. 2. For example, the number of external connections in the oldest subjects is several times smaller compared with the youngest. Since external links are longer than the internal, Fig. S1, the decreases in the external, and generally longer, links could be an effect of a same phenomenon targeting either longer or the external links.

We also checked to what extent the loss of tracts impacts the average length of the remaining tracts. To each link we assign as many tracts as given by its weight, each of them with a length equal to the mean of all the tracts. Results in Fig. 3 show that the mean and median length of the tracts decrease with aging, and

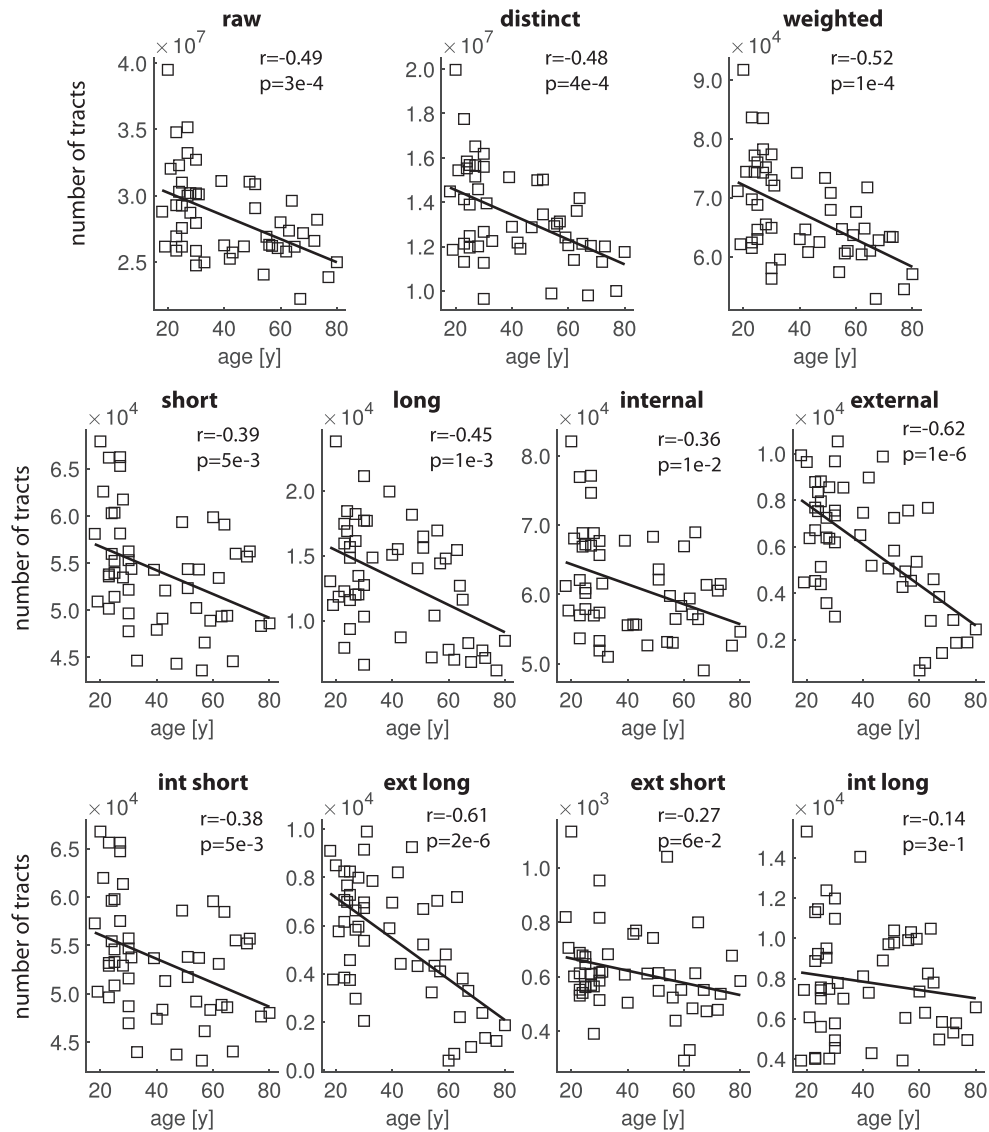


Fig. 2. Number of tracts per subject and their correlation with age. (top) Total number of raw counts (left), distinct connection counts (middle), and weighted distinct connection counts (right); and total number of distinct connection counts for (middle plots left to right) short, long, internal, and external links; and for (bottom plots left to right) internal short, external long, external short, and internal long links.

that the external and long links are mostly affected. It is worth noting that the internal links have longer mean than median values, indicating that they have asymmetric distribution with long outliers. For the external links on contrary, median and mean values are very close to each other. Short external links have more short outliers, and long external links have more long outliers that skew the means. These effects become stronger with aging, indicating that despite the significant decrease of the average length of the external links, the length of long and short external links are less affected. Instead, it is the loss of external long links, Fig. 2, that reduces the length of the remaining external and long connections.

Lobe-specific changes

The total number of tracts and their length was analyzed taking into account which lobes of the brain they connect. The frontal lobe is the most affected by the decrease of fiber counts, Table 1 (top), and within-lobe fibers have generally larger loss than those between. Regions of the cingulate preserve the internal tracts, while their connections to the frontal, occipital and parietal lobe

are significantly reduced. Besides the frontal, the number of internal tracts in the occipital and parietal lobe also experience strong negative relationship with aging. As for the between-lobes connections, those between temporal and occipital lobes are the most decreased with age.

Another aspect of the white matter loss is shown in Table 1 (bottom), where the loss of tracts on the level of lobes is analyzed between and within hemispheres. The strongest effects from within the lobes, Table 1, are shown to be mainly due to the loss of inter-hemispheric links, for the case of the frontal and parietal lobe, while the loss is quite homogeneous for the occipital lobe. As for the connectivity between the lobes, the decrease within the hemispheres is stronger. In this case the results are the same as for the short links, with parietal links to temporal and to the cingulate regions mostly affected, together with the occipital to temporal connections. On the other hand, frontal to parietal links are mostly affected by the inter-hemispheric connectivity loss between the different lobes.

We also analyzed whether the observed effects are identically distributed among the longer and the shorter links (see Table S1

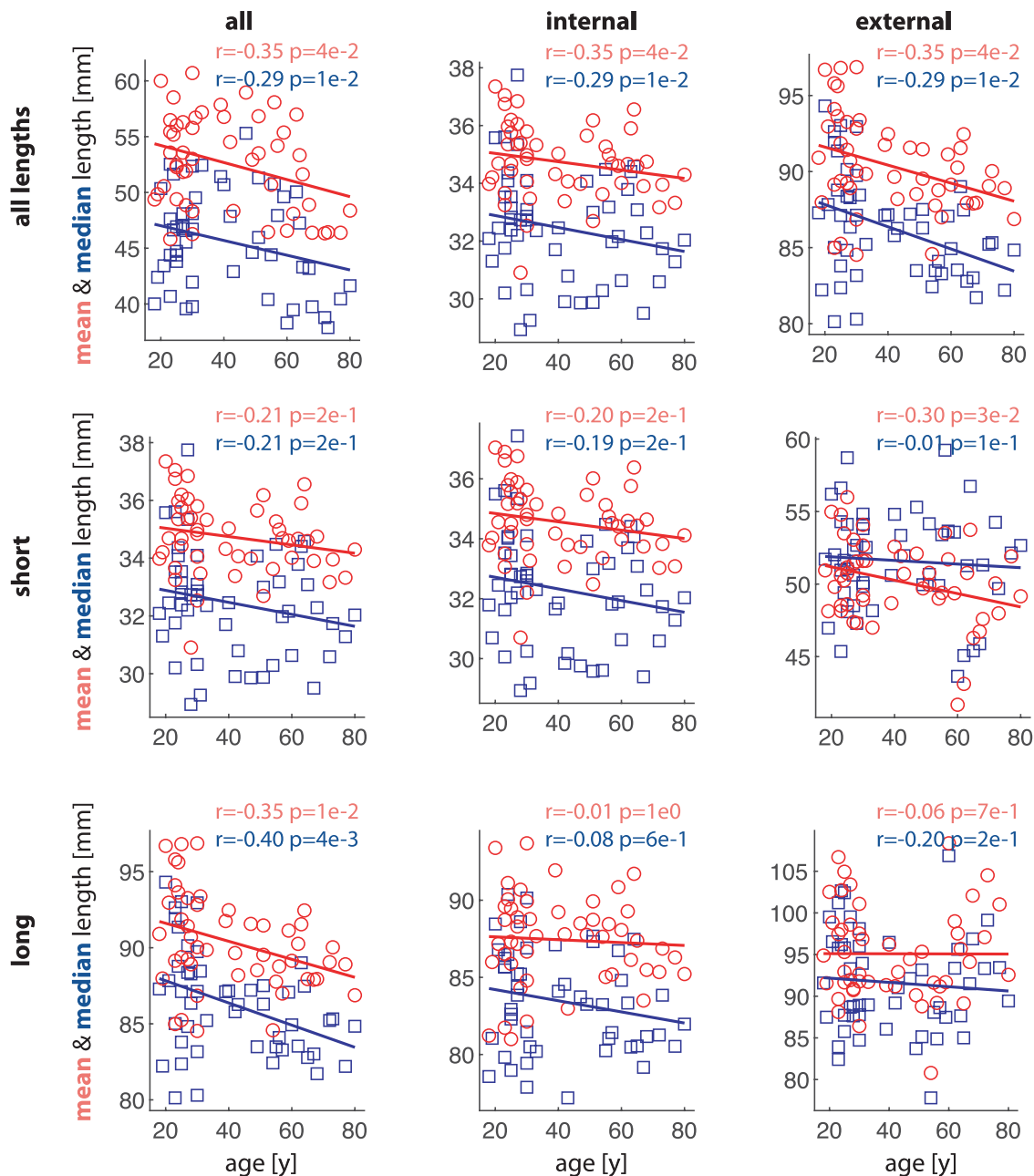


Fig. 3. Average tract lengths per subject and their correlation with age. Median (blue) and mean (red) track lengths for the whole brain (left column), internal links (middle column), and external links (right column) and for links of all lengths (top row), short links only (middle row) and long links only (bottom row).

Table 1. Correlation with age of number of tracts between lobes. Correlation coefficients with age and their P-values (in brackets) for the number of tracts in and between different lobes (top) and hemispheres (bottom). Statistically significant values ($P < 0.05$) are bold, values with $P < 0.005$, $P < 0.0005$, and $P < 0.00005$ are indicated with 1, 2, and 3 asterisks, respectively.

Lobes	Temporal	Cingulate	Frontal	Occipital	Parietal
Temporal	-0.25 (8.6e-2)	-0.16 (2.5e-1)	0.02 (8.9e-1)	-0.55*** (3.9e-5)	-0.43* (1.8e-3)
Cingulate	-0.16 (2.5e-1)	0.21 (1.4e-1)	-0.53** (9.0e-5)	-0.30 (3.1e-2)	-0.47* (5.3e-4)
Frontal	0.02 (8.9e-1)	-0.53** (9.0e-5)	-0.58*** (8.4e-6)	0.03 (8.3e-1)	-0.01 (9.2e-1)
Occipital	-0.55*** (3.9e-5)	-0.30 (3.1e-2)	0.03 (8.3e-1)	-0.53** (8.1e-5)	-0.24 (9.5e-2)
Parietal	-0.43* (1.8e-3)	-0.47* (5.3e-4)	-0.01 (9.2e-1)	-0.24 (9.5e-2)	-0.48* (4.8e-4)

(Continued)

Table 1. Continued

Lobes	Temporal		Cingulate		Frontal		Occipital		Parietal		
	left	right	left	right	left	right	left	right	left	right	
Temporal	left	-0.13 (3.7e-1)	-0.05 (7.6e-1)	0.18 (2.0e-1)	0.07 (6.1e-2)	-0.06 (6.9e-1)	-0.16 (2.8e-1)	-0.54*** (5.0e-5)	-0.15 (3.1e-1)	-0.35 (1.3e-2)	-0.26 (6.7e-2)
	right		-0.32 (2.4e-2)	0.24 (8.8e-2)	0.17 (2.3e-1)	-0.21 (1.4e-1)	0.11 (4.6e-1)	-0.19 (1.9e-1)	-0.38 (7.2e-3)	-0.36 (1.1e-2)	-0.39 (5.3e-3)
Cingulate	left		0.26 (7.2e-2)	0.05 (7.2e-1)	-0.43* (1.8e-3)	-0.39 (5.6e-3)	-0.38 (6.4e-3)	-0.35 (1.3e-2)	-0.45** (9.1e-4)	-0.12 (4.2e-1)	
	right			0.15 (3.1e-1)	-0.33 (2.0e-2)	-0.45** (1.2e-3)	-0.29 (3.8e-2)	0.01 (9.6e-1)	-0.15 (3.0e-1)	-0.38 (7.3e-3)	
Frontal	left				-0.22 (1.2e-1)	-0.54*** (5.3e-5)	-0.04 (8.0e-1)	0.03 (8.5e-1)	-0.04 (7.9e-1)	-0.47*** (4.9e-4)	
	right					-0.23 (1.0e-1)	-0.23 (1.1e-1)	0.06 (6.6e-1)	-0.38 (6.0e-3)	0.13 (3.8e-1)	
Occipital	left						-0.40* (3.7e-1)	-0.41* (2.9e-3)	0.02 (9.1e-1)	0.21 (1.5e-1)	
	right							0.51*** (1.5e-4)	-0.31 (3.0e-2)	-0.31 (3.0e-2)	
Parietal	left								-0.03 (8.3e-1)	-0.56*** (2.5e-5)	
	right									-0.16 (2.7e-1)	

in the [Supplementary Material](#)), with the division set at 70mm. Longer tracts are more affected than the short only for the links within the parietal and between the parietal and occipital lobe. Shorter tracts on the other hand are more contributing to loss of connectivity for the links connecting the cingulate with the frontal and parietal regions, as well as those between parietal and temporal lobes. For the other significant changes from [Table 1](#) (top), the effect is mostly equally affecting longer and shorter tracts.

Besides region-specific change in the total number of tracts, we also analyzed the relationship between age and mean of the inter- and intra-lobe tract lengths, since the overall length of tracts is also affected by aging, [Fig. 3](#). Comparing the obtained trends in [Table 2](#), with those for the number of tracts in [Table 1](#), we point to several features of the lobe-specific connectivity reorganization with aging. Tracts within the frontal lobe are again influenced the strongest, meaning that not only their number is mostly reduced compared with the other lobes, but their length decreases the most. The same is the case with the links within the parietal and between the parietal lobe and cingulate. Separate analysis for the long versus the short portions of the tracts (see [Tables S1–S2](#) in the [Supplementary Material](#)) reveals that for the within frontal and within parietal tracts, the reduction in length is due to the strong decrease of the longer tracts, despite the preserved length by the remaining long links. As for the parietal-cingulate links, their loss mainly affects the shorter ones, which become even shorter. It is interesting to note that temporal-cingulate links are the only one with significant increase of their average lengths, while their overall count also increases, but not significantly.

The loss of tracts is not necessarily related to the reduction of their length. For example, the tracts connecting the temporal with occipital and parietal regions preserve their mean length beside the strong decrease of their total count. Similarly, although the total number of tracts between occipital and the parietal lobe is not significantly reduced, there is a significant reduction in long tracts, [Table S1](#), which then leads to reduced mean length. When accounting for the hemispheres and lobes, the change in length is

generally smaller, [Table S3](#). The strongest decrease is observed for the inter-hemispheric links within the frontal lobe and frontal-cingulate. Interestingly, the length of inter-hemispheric frontal-parietal tracts are not particularly impacted besides the strong reduction in the overall connectivity, [Table 1](#). Similar patterns were found for the inter-hemispheric parietal, and for within occipital links.

Clustering

Possible changes in the clustering and modularity of the SC were investigated using Louvain modularity ([Blondel et al. 2008](#)) for weighted undirected links from the Brain Connectivity Toolbox ([Rubinov and Sporns, 2010](#)). The optimal number of clusters was set at 2, 3, 4 and 5 and even though the modularity decreased in all the studied cases, [Fig. S2](#), these were not statistically significant. For all but one subject the modularity decreases by increasing the number of partitions. Hence, for 49 of the subjects statistically significant highest modularity is achieved for 2 partitions. For 32 out of 50 subjects even without setting the initial division on hemispheres, this was found as the optimal (with highest modularity coefficient) in each of the 100 runs of the algorithm. In only 3 of the rest, the same resolution parameters for the hemispheric division did not yield higher modularity.

Similar results were observed for the modularity of weak, strong, short and long tracts, [Fig. S2](#). The modularity is mostly influenced by the strong links, so the modularity of these only are very similar to the case of the full connectome. Short links-only networks yield optimal hemispheric division for each of the subjects, while weak links give optimal modularity with 2 clusters for every subject, with hemispheric division being the most optimal for 45 of them. Long links on the other hand do not exclusively produce significantly smaller modularity for larger partitions, as it would have been expected from the distribution of the tract lengths, [Fig. S1](#) and also ([Petkoski et al. 2016, 2018](#)), which show that most of the inter-hemispheric tracts are long, compared with the median. However, due to the misrepresentation of the inter-hemispheric

Table 2. Correlation with age of mean length of tracts between lobes. Correlation coefficients with age and their P-values (in brackets) for the mean length of tracts in and between different lobes. Statistically significant values ($P < 0.05$) are bold, values with $P < 0.005$ and $P < 0.0005$ are indicated with 1 and 2 asterisks, respectively.

Lobes	Temporal	Cingulate	Frontal	Occipital	Parietal
Temporal	-0.24 (9.9e-2)	0.30 (3.6e-2)	-0.09 (5.5e-1)	-0.11 (4.3e-1)	0.04 (8.0e-1)
Cingulate	0.30 (3.6e-2)	0.08 (5.7e-1)	-0.14 (3.3e-1)	-0.16 (2.7e-1)	-0.40* (4.5e-3)
Frontal	-0.09 (5.5e-1)	-0.14 (3.3e-1)	-0.50** (2.0e-4)	-0.04 (7.8e-1)	0.20 (1.6e-1)
Occipital	-0.11 (4.3e-1)	-0.16 (2.7e-1)	-0.04 (7.8e-1)	-0.28 (5.2e-2)	-0.30 (3.3e-2)
Parietal	0.04 (8.0e-1)	-0.40* (4.5e-3)	0.20 (1.6e-1)	-0.30 (3.3e-2)	-0.45* (1.0e-3)

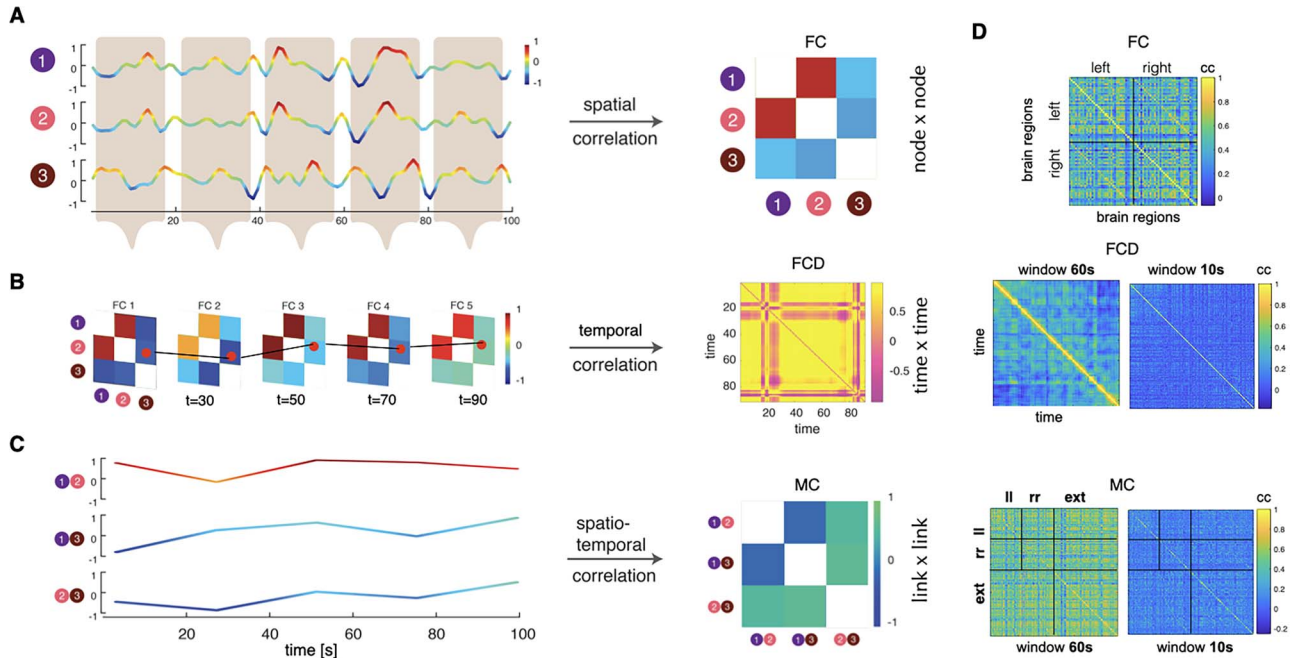


Fig. 4. From static to dFC. A) Traditionally, correlations between neural activity time-series of N different brain region nodes are averaged over long times and compiled into the entries FC_{ij} of a static $N \times N$ FC matrix (right). B) Sliding windows of a shorter temporal duration, it is possible to estimate a stream of time-resolved $FC(t)$ networks, so-called dFC stream. The degree of similarity (inter-matrix correlation) between $FC(t)$ networks observed at different times is then represented into a dFC matrix. C) Alternatively, one can consider each individual FC link as a dynamic variable FC_{ij} attached to the graph edge between two regions i and j . Generalizing the construction of the FC matrix in panel (A), we can thus extract a $N(N - 1) \times N(N - 1)$ matrix of covariance between the time-courses of different FC_{ij} links, giving rise to the MC matrix. (see Arbabyazd et al. (2020) for more details). (D) Example of empirical FC, FCD, and MC for the first subjects, with the latter two calculated for window sizes of 60 and 10 seconds, and overlap of 58 and 8, respectively. Links in the MC matrix rows and columns are ordered starting from internal left hemispheric, internal right hemispheric and external (inter-hemispheric).

tracts with diffusion tensor imaging (DTI) (Reveley et al. 2015, Zalesky et al. 2016), the intra-hemispheric long links are still of a similar size as the inter-hemispheric links. This still results in high intra-hemispheric connectivity, and hence, high modularity for hemispheric division.

Taken together with the distribution of the track lengths, Fig. S1, and the highest modularity for the hemispheric division, suggest that the spatio-temporal structural architecture can be approximated into two modules corresponding to the hemispheres. Correspondingly, measures of the network dynamics are expected to distinguish between intra- and inter-hemispheric data features.

Functional reorganization

Static FC, Fig. 4(A), decreases with age for the internal and external links of every lobe, but none of them is statistically significant (Table S4 top). Similarly, the FC decreases without statistical significance for the resting state networks (Table S4 bottom).

To go beyond the static data features, we analyzed the alterations with age in the dynamics of FC, as captured by dFC and

MC (Arbabyazd et al. 2020), Fig. 4(B). We focused on the dFC walk paradigm, as introduced by Battaglia et al. (2020). In short, relatively small variations of FC from one observation time to the next result in shorter flight lengths and more extensive network reconfigurations than in larger flight lengths. We characterize this temporal evolution of the FC by the mean of the dFC. Smaller mean of dFC corresponds to a more dynamically fluid brain, which quicker reconfigures its dynamics.

For the spatial aspects of the dFC we analyzed MC (Lombardo et al. 2020). It captures correlations between the links, Fig. 4(C), which are grouped in different modules depending on whether they are inter- or intra-hemispheric, where the latter are further divided by the hemispheres. Thus, we analyzed dynamics associated with five spatially separate modules: left-left to left-left, left-left to right-right, right-right to right-right, left-right to left-right, and intra-hemispheric (left-left and right-right) to inter-hemispheric (left-right), Fig. 4(D).

Fluidity of dFC showed a significant decrease with aging as captured by the increase of the mean non-overlapping off-diagonal dFC (further simply referred as mean dFC), and hence decrease of

the mean dFC velocity, as already reported (Battaglia et al. 2020). This relationship is increasing and becoming more significant for smaller lengths of the sliding window, Fig. 5. Similar trends are also observed for the median and mode of dFC, and only for the short sliding windows these are accompanied by increases of the variance and kurtosis, Fig. S3.

Even more significant changes were observed for the higher order interactions of dFC, as captured by the MC, Fig. 5. These show a very significant increase of the range and STD of MC, which point to increased variations of spatial covariations. The effects were also systematically more pronounced for smaller windows. Here we were able to analyze the spatial component of the dynamical connectivity, revealing that the trends are generally preserved among all pairs of links. Nevertheless, interactions involving inter-hemispheric links are slightly stronger affected, followed by the MC between the intra-hemispheric links and between the inter- and intra-hemispheric links.

BNM for the dependence of the function from structure

To mechanistically analyze the effects of the aging-related SC reorganization to neuronal activity, we constructed a brain network model. From the neuronal activity that operates at EEG frequency bands, we simulated BOLD time-series and repeated the same analysis as for the empirical recordings. We built the BNM using Kuramoto oscillators (Kuramoto, 1984) with explicit heterogeneous time-delays (Petkoski et al. 2018). Beside its simplicity and representing highly idealized system, the model can nonetheless exhibit rather non-trivial collective dynamics that could map different states of the brain (Breakspear et al. 2010; Cabral et al. 2011; Sheppard et al. 2013; Petkoski et al. 2018). In its current implementation, its simplicity allows it to only account for the impact of the spatio-temporal structure of the connectivity to the emergent dynamics.

Having fixed noise and natural frequencies, as well as individual connectivity, we performed parametric exploration of the global coupling and conduction velocity, as the only free parameters of the model. This allowed us to test several hypotheses. For the global coupling, we explored two strategies: (i) constant scaling for each subject, which implies a very strong impact of the connectivity loss to the dynamics and (ii) subject-specific scaling proportional to the mean strength of the weights, which implies compensatory mechanisms for each subject. The first strategy proportionally accounts for the connectivity loss and it leads to very different dynamics between subjects, because the mean values of the weights, which mainly constrain the network dynamics (Rodrigues et al. 2016) differ between subjects by as much as 100%, as seen in Fig. 2.

The second approach decreases the influence of the SC, and practically compensates its loss by bringing the dynamical working point of the subjects in the same range. This is supported by the fact that all the subjects are healthy and in a similar dynamical state. Hence, it is not expected for the large-scale dynamical properties between them to deviate too strongly, as also visible in the empirical data. Moreover, the effect of subject-specific spatio-temporal structure is still fully shaping the observed dynamics.

For the conduction velocity, we also adopted 2 strategies: (i) fixed velocity for each subject that does not explicitly takes into account the effects of demyelination with aging, which are not captured by the connectome, and (ii) decreasing velocity with age, which assumes that not all of the aspects of the demyelination are fully captured by the SC through changes in the fractional anisotropy and henceforth weights, but increased propagation

time at the existing links should be explicitly taken into account. In the case of age-dependent conduction velocity, it is calculated as

$$v_{subj} = v_0 - \frac{age_{subj} - \min(age)}{\max(age) - \min(age)} \Delta v.$$

The last hypothesis that we checked with the BNM, was whether the decomposition of the time-delays into the hemispheric modes (Petkoski et al. 2016, 2018) is sufficient to capture the main data features of the dynamics at time-scales of BOLD.

Simulations for dFC reveal that there is a relatively wide parameter range for the global coupling scaled individually, and for conduction velocities linearly decreasing with age, where the average statistics of dFC is in agreement with the empirical results, Fig. 6(A). Significant increase with age for the means of dFC occurs for all 4 window lengths, and not only for the full model, but also when the spatially reduced delay matrices are used, Fig. S7. More importantly, it is not only the same trend with age that appears statistically significant, but that is also the case for the subject specific metrics. Assuming global instead of individualized scaling for the global coupling, generally reverses the trends in the statistics of dFC, and the same is the case for constant conduction velocity. Same parameter sweep for the global coupling was also run for propagation velocities of 2m/s and 5m/s, which for both models showed qualitatively similar patterns as for 3.3m/s, see Fig. S7, but weaker agreement with the empirical results. For the case with no delays, the results do not show any significant trends with age, nor significant correlation with empirical, subject-specific results.

The spatial aspect of dFC is captured by the statistics of MC that is shown in Fig. 6(B-C). The strongest age-related patterns of the range and the STD of MC are well captured by the model (and by its reduced version, Fig. S6) around the same working points as for FCD. Significant correlations again appear also for the individualized dynamics, in addition to the general age-related trends. Unlike the results for FCD, here significant correlations with the aging trends also can occur for the case of age-independent propagation velocity, or global scaling, though for fewer parameters, and never for the same working point consistently across the metrics.

Finally, it is worth noting that fluidity of the dynamics at time-scales observed in dFC is the largest for global coupling that showed the best match with the data, as it can be seen by the values of STD and range of FCD (Fig. S5(e-h)). Even though these are dependent on the window sizes, the highest predictive value of the model is observed around the values of global couplings which maximize the variance of dFC. This has been hypothesized to be the working point of the brain dynamics (Rabuffo et al. 2021), and in our case, this optimal dynamical range also overlaps with the working point where the model reaches the highest predictive value for the static FC (Fig. S5(i-j)). Interestingly, on the fast time scales of the oscillators, this does not correspond to the range with highest metastability at the brink of synchronization (Fig. S5(c-d)), but to the synchronized regime (Fig. S5(a-b)).

Discussion

In this work we identify the significant changes in the dynamics of brain FC, as reflected in dFC and MC metrics for the dynamical reconfigurations, and we apply a BNM to identify which aspects of the spatiotemporal reorganization of the brain structure with the aging could be responsible for the latter dynamical alterations.

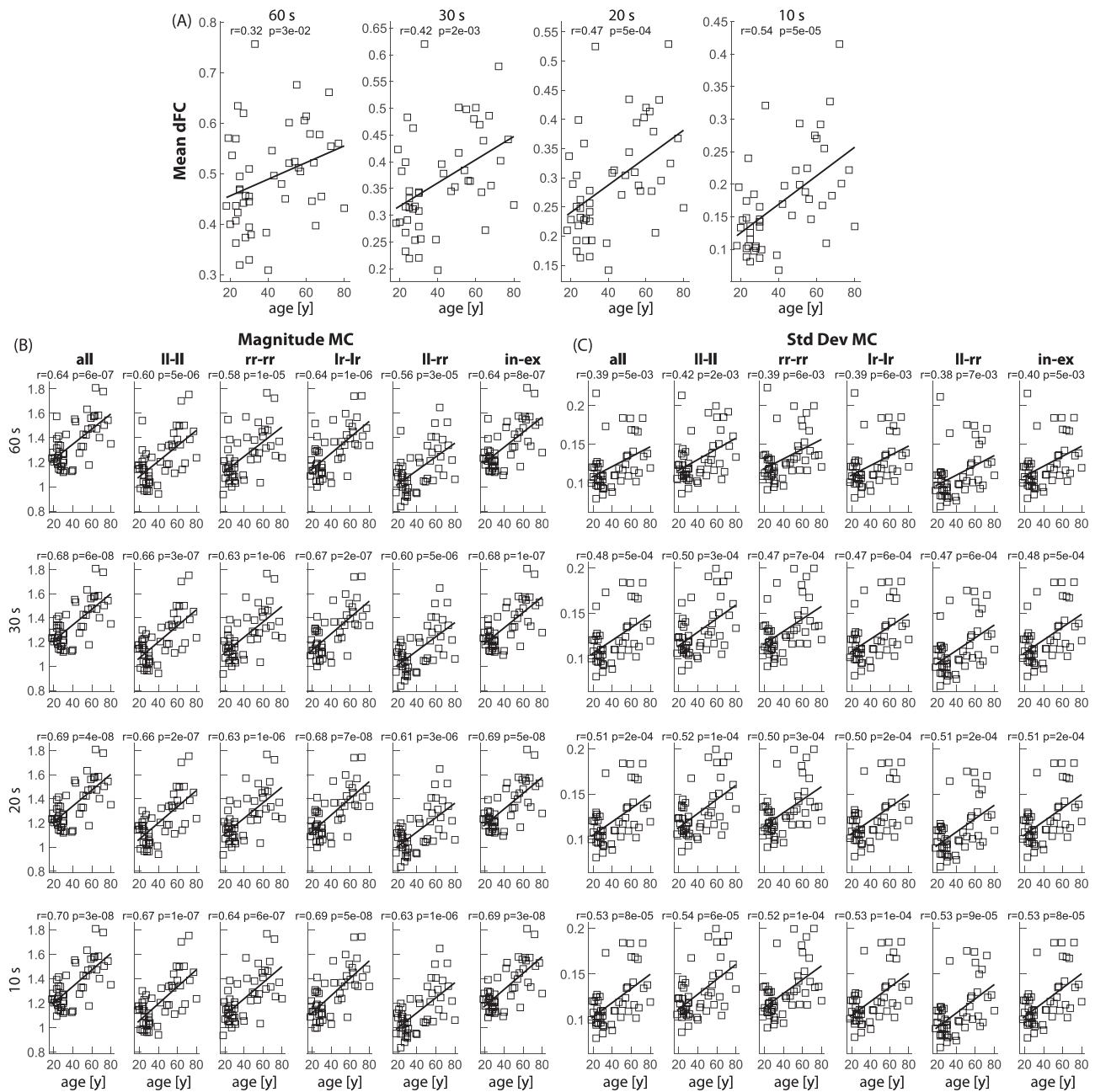


Fig. 5. Age-dependent subject-specific dFC and MC. Scatter plots of mean dFC (A) and magnitude (B) and STD (C) of different spatial components of the empirical MC against subjects' age for different sizes of the sliding windows. (ll = left-left, rr = right-right, lr = left-right, ext = - external/inter-hemispheric, int = - internal/intra-hemispheric).

SC alterations with age

More than half of the human brain volume is made up of white matter: regions where axons are coated in myelin, which primarily functions to increase the conduction speed of axon potentials. Myelin sheaths are produced and maintained by oligodendrocytes, whose capacity in doing so is reduced with aging (Sams, 2021). This, however, cannot be retrieved with neuroimaging, causing a generally neuron-centric approach in the research of non-pathological brain aging mechanisms. Due to this limitation, we describe only the changes in brain structure as captured by tractography, but in the causal BNM we explicitly account for the impact of the demyelination on the conduction velocity.

Age-related loss of brain's structural connectivity has been of interest in many studies (Betz et al. 2014; Lim et al. 2015; Perry et al. 2015) that, nevertheless, overlooked the impact on the tract lengths and their spatial distribution, which are of focus here. Topological organization of the white matter connectivity across the human lifespan is characterized by a decrease in the global network properties, such as the connectivity strength, starting from the third decade (Coupé et al. 2017; Zhao et al. 2015). This is confirmed with our results for the decrease in SC. The loss of white matter connectivity is especially pronounced for the inter-hemispheric links, as already reported (Puxeddu et al. 2020), causing the average length of the remaining tracts to decrease with age, because the inter-hemispheric links are on average longer.

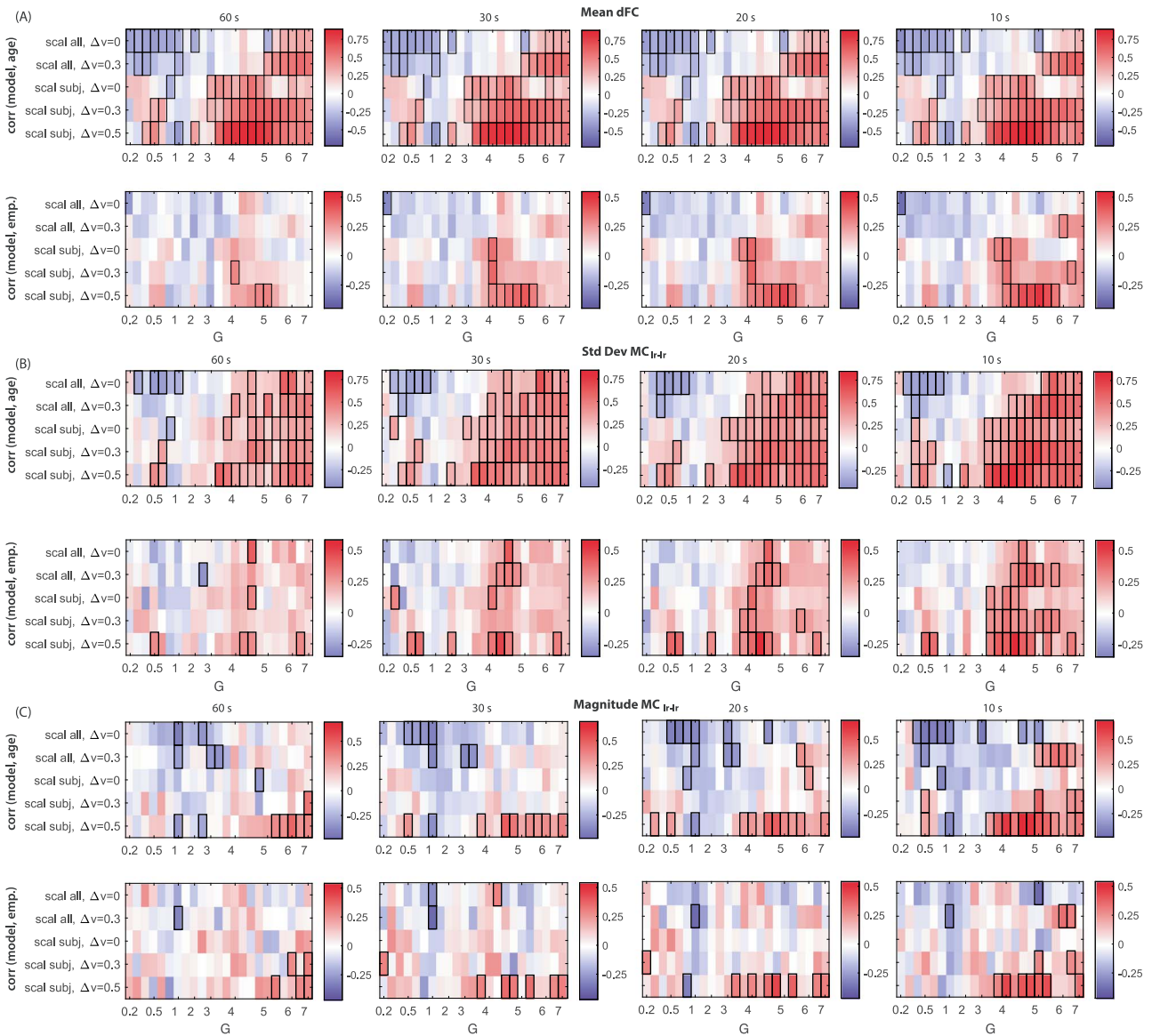


Fig. 6. Model fit for the empirical dFC and MC. Correlation between simulated data features with age, and with the subject specific empirical results. (A) The mean of the off-diagonal dFC is used for the temporal aspects of dynamical reconfiguration, and for the spatial it is (B) STD between MC of inter-hemispheric links (upper plots) and (C) range of MC values between the links in the left and in the right hemisphere (lower plots). The results are shown for different size of the moving window (60s, 30s, 20s, and 10s) levels of global coupling G , scaling for the cohort (identical scaling for each subject indicated with *scal all* and subject specific scaling dependent on their mean connectivity indicated with *scal subj*) and age-dependent linear decrease of the conduction velocity Δv . Statistically significant correlations are indicated with black rectangles. Parameters: conduction velocity $v_0 = 3.3m/s$, natural frequency $f = 10Hz$, noise intensity $D = 1$.

The frontal lobe is the strongest affected area by the loss of fiber counts, Table 1, in agreement with the literature (Peters, 2006, Gunning-Dixon et al. 2009). Similarly strong loss is observed in the occipital lobe, but this is more equally affecting intra- and inter-hemispheric links, hence having much smaller impact on the tract lengths. Even though we found within-lobe fibers to be more affected than those between lobes, Table 1, the modularity is still generally stable, in line with similar studies (Lim et al. 2015).

Many studies indirectly point to the decrease of white matter fibers in the frontal regions by showing strong negative relationship with functional anisotropy and age, that is especially prominent in the frontal lobe (Grieve et al. 2007; Inano et al. 2011; Billiet et al. 2015). Most of the these works (Grieve et al. 2007; Inano et al. 2011; Mädler et al. 2008) also measured axonal and radial diffusion, and related the trends in those measures to the demyelination, as indicated by the measurements of myelin

water fraction. However, there are also some contradicting studies (Billiet et al. 2015), which although observed the decrease of fractional anisotropy with aging, did not find significant difference in myelin water fraction. We did not recover myelination or other related metric, but instead using the BNM we found that model's predictability is increased if a reduction of conduction velocity due to hypothesized demyelination is assumed to occur linearly with age.

dFC alterations with age

It is now a widely recognized concept in the study of dynamics of the human brain network, that FC is not static, but changes its pattern over time, even during rest. The possibility of studying these dynamics through analysis of neuroimaging data has catalyzed substantial interest in methods that estimate time-resolved fluctuations in FC (Lurie et al. 2020). In the context of

aging, temporal variations of the resting-state showed decrease of FC variation for the inter-network connections (Chen et al. 2017). Dynamic FC tends to slow down with increasing age (Battaglia et al. 2020), and cognitive performance in healthy older adults relates to spontaneous switching between states of FC during rest, as captured by dFC (Cabral et al. 2017). Also, lower metastability at slow time-scales of BOLD activity is associated with higher age (Escrachs et al. 2020), which is in agreement with the functional benefits of greater variability in neural systems, including flexibility/adaptability, heightened dynamic range, Bayesian optimality, and multi-stability (Garrett et al. 2011; Sleimen-Malkoun et al. 2014).

Here, first we showed that several metrics derived on static FC do not correlate with the age, in line with the generally low predictive power of FC (Domhof et al. 2021). Often the simulated FC that fits best to the same subject's empirical FC may not necessarily be the same simulated FC (Triebkorn et al. 2020). Next, we focused our analysis on the temporal aspects of dFC and the spatial aspects of covariation between FC links. The former confirmed the slowing down of dFC (Battaglia et al. 2020), which is accelerated at shorter time-scales, as observed from the mean dFC calculated at shorter windows. Interestingly, the variance of dFC is less affected, and only starts to significantly increase at faster time-scales.

The dFC is highly dependent on the sliding windows (e.g. notice the overall decrease in correlation values with the decrease of the window size). To avoid this we have carried out the analysis on different sized windows, thus further demonstrating the robustness of the observed features. Another possibility would have been to use an unsupervised data-driven approach (Sastry et al. 2022).

Age-related changes are even stronger for the covariations between FC links, as captured by spatial components of MC. Here, it is not the means that are mostly affected, but the variance and range of MC, which very significantly increase with age. Larger impact is still present for shorter time-scales, although to a smaller extent. Spatially speaking, the trends are strongest for the covariation of inter-hemispheric links between themselves (even though the inter-hemispheric static FC is unaffected), and for the internal links of hemispheres between each other. These results point for the first time that taking into account the spatial aspects of the dFC through higher order interactions, could serve as a better and more robust biomarker for aging. This is to be expected also due to the large spatial heterogeneity of the white-matter loss, which nevertheless does not result in observable changes in the respective static FC metrics. A possible reason for this is the fact that FC by definition averages out nonlinearities in the dynamics, which are highly non-stationary (Heitmann and Breakspear, 2017; McIntosh and Jirsa, 2019).

Linking the structure and the function

Age-related alterations in brain structure and function have been linked to age-related cognitive decline, although challenges still remain (Hedden et al. 2016). Sources of heterogeneity are not fully understood, but seem to be associated with different neurobiological substrates (loss of white matter tracts and demyelination), and single-cohort designs might be optimal in reducing the sources of interindividual variation that may be unrelated to age (Zuo et al. 2016). Current models indicate that structure and function are significantly correlated, but the correspondence is not perfect because function reflects complex multisynaptic interactions in structural networks (Suárez et al. 2020). This has been demonstrated also in the respect with aging (Zimmermann et al. 2018), where SC and FC each show unique and distinct

patterns of variance across subjects, and variability of FC alterations is especially high across older adults (Stumme et al. 2020). Therefore, function cannot be directly estimated from structure, but must be inferred by mechanistic models, which can causally test the higher-order interactions (Schirner et al. 2018, Courtiol et al. 2018), and offer higher explanatory value compared with the data-driven methods (Jockwitz et al. 2017). It was already shown that a specific pattern of SC/FC coupling predicts age more reliably than does region wise SC, or FC decrease alone (Zimmermann et al. 2016), but the dependence between the SC age-related changes and the FC reorganizations are still ambiguous. This indicates that the impact that SC has on brain dynamics needs to be investigated beyond the FC (Triebkorn et al. 2020).

Choosing sine coupling is the simplest form for the phase reduction of weakly coupled oscillators (Kuramoto, 1984). The coupling functions in real systems often involves different frequency bands (Jirsa and Müller, 2013; Stankovski et al. 2017b) and take complex forms (Stankovski et al. 2017), which can be of crucial importance for regulating biological oscillations (Stankovski et al. 2016). Another step to make the model more realistic would be through explicit inclusion of the sources of variability of the model parameters (Petkoski et al. 2012). These could be contributing to the slow rhythms at the ranges captured by dFC. Notably, this has been demonstrated for the cardiovascular oscillations (Musizza et al. 2007; Stankovski et al. 2016) and for the thalamus and other subcortical structures that shape the dynamical landscape of the cortical activity (Shine et al. 2019; Taylor et al. 2022). In addition, biasing the parameters of BNM with structural heterogeneity has been shown to increase the predictive power of the models of the resting state (Kong et al. 2021; Schirner et al. 2018), whereas data-driven approaches have identified good match of inferred regional parameters and the structural heterogeneity (Sip et al. 2021).

Compensation (Lövdén et al. 2010) of the brain is probably among the major causes that impede establishing individualized SC/FC link with aging. Another reason could be that time-delays are often ignored, and they still cannot be retrieved on individual level, but tract lengths are used as a proxy (Sanz-Leon et al. 2015). This, however, cannot capture the important effects that demyelination might have on increasing the propagation delays (Sorrentino et al. 2022). Scaffolding is a normal process present across the lifespan that involves use and development of complementary, alternative neural circuits to achieve a particular cognitive goal (Park and Reuter-Lorenz, 2009). Hence, the behavioral performance in older adults is often hypothesized to depend on keeping some quantity invariant through compensation in another. Preservation of neuronal synchrony in aging through enhancing inter-areal coupling has been suggested as one such example (Pathak et al. (2022b)). Here, we do not investigate a functional feature that is kept invariant. Instead, through a battery of metrics we report the functional reorganization associated with healthy aging, and we demonstrate that the increase of global coupling, together with the demyelination, are necessary for this to occur in the brain model. On the other hand, the structural connectivity is significantly decreased in aging, implying that the increased global coupling compensates the lost connectivity. This is perfectly plausible from the dynamical viewpoint, but it is still unknown which biophysical mechanism could be responsible for the shift in the global coupling. This is purely phenomenological parameter, which has been also shown to be important in setting the working point in the case of epilepsy (Courtiol et al. 2022). Most likely, it is linked to the regulatory changes in neuromodulation that are missing in our model, in

particular, the aging-related increase of dopamine synthesis capacity (Berry et al. 2016).

The model shows statistically significant individualized predictive value for the most significant dFC and MC data features. This is observed only if: (i) dynamical compensation is assumed through the global effective coupling that is identical across subjects (by normalizing each connectome with the individualized mean connectivity) and (ii) conduction velocity is linearly decreased with aging to account for the demyelination that is not accounted in the weights and lengths of the individualized connectome. The results hold even if the spatio-temporal connectivity is spatially decomposed (Petkoski et al. 2016; 2018; Petkoski and Jirsa, 2019), such that only lumped intra and inter-hemispheric delays are taken into account. The latter is supported by the results for the SC alterations, which indeed show that the strongest decrease with aging is observed for the inter-hemispheric tract lengths. Interestingly, the best fit for dFC and MC is obtained at the working point that maximizes the variability of dFC, as observed through its variance, as it has been independently used as a criterion for the healthy homeostasis of the brain (Rabuffo et al. 2021; Triebkorn et al. 2020). This holds for both, the original and reduced model.

Limitations of the study

Using larger cohorts that become more available, such as 1000Brains (Caspers et al. 2014), would improve the reliability of the obtained results. Handling larger datasets would, however, require using digital research platforms such as EBRAINS that allows integration and accessibility of those datasets together with simulation engines (Schirner et al. 2022). Parcellation-induced variation of empirical and simulated brain connectomes at group and subject levels is another issue that needs to be considered (Domhof et al. 2021). Nevertheless, most of our findings for the structure and function, and for their link with the model, independently and robustly show statistically significant trends with age, and individually. This gives us confidence in the reported changes, and in the mechanisms linking them, which we recovered on an individualized level for the first time. To compensate for the focus on a single cohort of a modest size, with the model and with the applied hypotheses we have tried to be as general and unbiased as possible. We are covering static and dynamical data features, as well as higher order interactions, for a wide range of the global couplings, which cover different dynamical regimes—from weak synchronization, through high metastability to high synchronization.

Interestingly, decomposition of time-delays in the reduced model probably works because using homogeneous conduction velocities is already introducing bias for the delays. As such, the main modes of the delays were shown in silico to contain sufficient predictive value (Petkoski et al. 2018; Petkoski and Jirsa 2019). The conduction velocities of action potentials differ could be between 0.1 m/s and 10 m/s (Waxman, 1980), depending on the axonal diameter and the presence of a myelin sheath, but obtaining reliable individualized maps on whole-brain level is still impossible. Importantly, however, Caminiti et al. (2013) found that the spectrum of tract lengths obtained with MRI closely matches that estimated from histological reconstruction of axons labeled with an anterogradely transported tracer. They also measured conduction velocity of myelinated axons in the human brain that were between 6 and 10 m/s. It has also been reported that similar overall population of myelinated to nonmyelinated axons can be found in corpus callosum of different species (Olivares et al. 2001), with the latter generally having velocity <1m/s. All these

indicates that better estimates of the time-delays (Lemaréchal et al. 2021), especially if they are personalized (Sorrentino et al. 2022), are expected to improve the predictive power of any whole-brain model.

Supplementary material

Supplementary material is available at *Cerebral Cortex* online.

Acknowledgments

In addition, PR acknowledges support by ERC Consolidator 683049; German Research Foundation SFB 1436 (project ID 425899996); SFB 1315 (project ID 327654276); SFB 936 (project ID 178316478), SFB-TRR 295 (project ID 424778381); SPP Computational Connectomics RI 2073/6-1, RI 2073/10-2, RI 2073/9-1; Berlin Institute of Health and Foundation Charité, Johanna Quandt Excellence Initiative.

Funding

This research was supported by the European Union's Horizon 2020 Research and Innovation Programme under grant agreement No. 945539 (SGA3) Human Brain Project and by grant agreement No. 826421 Virtual Brain Cloud.

Conflict of interest statement: None declared.

References

- Acebrón JA, Bonilla LL, Vicente CJP, Ritort F, Spigler R. The Kuramoto model: a simple paradigm for synchronization phenomena. *Rev Mod Phys.* 2005;77(137–185):0306625.
- Allegra Mascaro AL, Falotico E, Petkoski S, Pasquini M, Vannucci L, Tort-Colet N, Conti E, Resta F, Spalletti C, Ramalingasetty ST, et al. Experimental and computational study on motor control and recovery after stroke: toward a constructive loop between experimental and virtual embodied neuroscience. *Front Syst Neurosci.* 2020;14:1–34.
- Arbablyazd LM, Lombardo D, Blin O, Didic M, Battaglia D, Jirsa V. Dynamic functional connectivity as a complex random walk: definitions and the dFCwalk toolbox. *MethodsX.* 2020;7:101168.
- Baltes PB, Lindenberger U. Emergence of a powerful connection between sensory and cognitive functions across the adult life span: a new window to the study of cognitive aging? *Psychol Aging.* 1997;12:12.
- Bassett DS, Sporns O. Network neuroscience. *Nat Neurosci.* 2017; 20:353–364.
- Battaglia D, Boudou T, Hansen EC, Lombardo D, Chettouf S, Daffertshofer A, McIntosh AR, Zimmermann J, Ritter P, Jirsa V. Dynamic functional connectivity between order and randomness and its evolution across the human adult lifespan. *NeuroImage.* 2020;222:117156.
- Berry AS, Shah VD, Baker SL, Vogel JW, O'Neil JP, Janabi M, Schwimmer HD, Marks SM, Jagust WJ. Aging affects dopaminergic neural mechanisms of cognitive flexibility. *J Neurosci.* 2016;36: 12559–12569.
- Bethlehem RA, Seidlitz J, White SR, Vogel JW, Anderson KM, Adamson C, Adler S, Alexopoulos GS, Anagnostou E, Areces-Gonzalez A, et al. Brain charts for the human lifespan. *Nature.* 2022;604: 525–533.
- Betzl RF, Byrge L, He Y, Goñi J, Zuo XN, Sporns O. Changes in structural and functional connectivity among resting-state networks across the human lifespan. *NeuroImage.* 2014;102:345–357.

- Billiet T, Vandenbulcke M, Mädler B, Peeters R, Dhollander T, Zhang H, Deprez S, Van den Bergh BRH, Sunaert S, Emsell L. Age-related microstructural differences quantified using myelin water imaging and advanced diffusion MRI. *Neurobiol Aging*. 2015;36:2107–2121.
- Blondel VD, Guillaume JL, Lambiotte R, Lefebvre E. Fast unfolding of communities in large networks. *J Stat Mech*. 2008;10:P10008.
- Breakspear M, Heitmann S, Daffertshofer A. Generative models of cortical oscillations: neurobiological implications of the kuramoto model. *Front Hum Neurosci*. 2010;4:190.
- Burke SN, Barnes CA. Neural plasticity in the ageing brain. *Nat Rev Neurosci*. 2006;7:30–40.
- Cabral J, Hugues E, Sporns O, Deco G. Role of local network oscillations in resting-state functional connectivity. *NeuroImage*. 2011;57:130–139.
- Cabral J, Vidaurre D, Marques P, Magalhães R, Silva Moreira P, Miguel Soares J, Deco G, Sousa N, Kringelbach ML. Cognitive performance in healthy older adults relates to spontaneous switching between states of functional connectivity during rest. *Sci Rep*. 2017;7:1–13.
- Caminiti R, Carducci F, Piervincenzi C, Battaglia-Mayer A, Confalone G, Visco-Comandini F, Pantano P, Innocenti GM. Diameter, length, speed, and conduction delay of callosal axons in macaque monkeys and humans: comparing data from histology and magnetic resonance imaging diffusion tractography. *J Neurosci*. 2013;33:14501–14511.
- Caspers S, Moebus S, Lux S, Pundt N, Schütz H, Mühleisen TW, Gras V, Eickhoff SB, Romanzetti S, Stöcker T, et al. Studying variability in human brain aging in a population-based German cohort—rationale and design of 1000brains. *Front Aging Neurosci*. 2014;6:149.
- Chen Y, Wang W, Zhao X, Sha M, Liu Y, Zhang X, Ma J, Ni H, Ming D. Age-related decline in the variation of dynamic functional connectivity: a resting state analysis. *Front Aging Neurosci*. 2017;9:203.
- Costa M, Goldberger AL, Peng CK. Multiscale entropy analysis of complex physiologic time series. *Phys Rev Lett*. 2002;89:068102.
- Coupé P, Catheline G, Lanuza E, Manjón JV, Initiative ADN. Towards a unified analysis of brain maturation and aging across the entire lifespan: a MRI analysis. *Hum Brain Mapp*. 2017;38:5501–5518.
- Courtiol J, Perdakis D, Petkoski S, Müller V, Huys R, Sleimen-Malkoun R, Jirsa VK. The multiscale entropy: guidelines for use and interpretation in brain signal analysis. *J Neurosci Methods*. 2016;273:175–190.
- Courtiol J, Guye M, Bartolomei F, Petkoski S, Jirsa VK. Dynamical mechanisms of interictal resting-state functional connectivity in epilepsy. *J Neurosci*. 2020;40:5572–5588.
- Deco G, Jirs V, McIntosh AR, Sporns O, Kötter R. Key role of coupling, delay, and noise in resting brain fluctuations. *Proc Natl Acad Sci U S A*. 2009;106:10302–10307.
- Deco G, Jirsa VK, McIntosh AR. Emerging concepts for the dynamical organization of resting-state activity in the brain. *Nat Rev Neurosci*. 2011;12:43–56.
- Desikan RS, Ségonne F, Fischl B, Quinn BT, Dickerson BC, Blacker D, Buckner RL, Dale AM, Maguire RP, Hyman BT, et al. An automated labeling system for subdividing the human cerebral cortex on MRI scans into gyral based regions of interest. *NeuroImage*. 2006;31:968–980.
- Domhof JW, Jung K, Eickhoff SB, Popovych OV. Parcellation-induced variation of empirical and simulated brain connectomes at group and subject levels. *Netw Neurosci*. 2021;5:798–830.
- Duffy FH, Mcanulty GB, Albert MS. Effects of age upon interhemispheric EEG coherence in normal adults. *Neurobiol Aging*. 1996;17:587–599.
- Ermentrout B, Wechselberger M. Canards, clusters, and synchronization in a weakly coupled interneuron model. *SIAM J Appl Dyn Syst*. 2009;8:253–278.
- Escrachs A, Biarnes C, Garre-Olmo J, Fernández-Real JM, Ramos R, Pamplona R, Brugada R, Serena J, Ramió-Torrentà L, Coll-De-Tuero G, et al. Whole-brain dynamics in aging: disruptions in functional connectivity and the role of the rich club. *Cereb Cortex*. 2020;31(5):2466–2481.
- Faes L, Marinazzo D, Stramaglia S. Multiscale information decomposition: exact computation for multivariate Gaussian processes. *Entropy*. 2017;19:1–18 1706.07136.
- Friston KJ. Functional and effective connectivity: a review. *Brain Connectivity*. 2011;1:13–36.
- Friston KJ, Harrison L, Penny W. Dynamic causal modelling. *NeuroImage*. 2003;19:1273–1302.
- Garrett DD, Kovacevic N, McIntosh AR, Grady CL. The importance of being variable. *J Neurosci*. 2011;31:4496–4503.
- Ghosh A, Rho Y, McIntosh AR, Kötter R, Jirsa VK. Noise during rest enables the exploration of the brain's dynamic repertoire. *PLoS Comput Biol*. 2008;4:e1000196.
- Grieve SM, Williams LM, Paul RH, Clark CR, Gordon E. Cognitive aging, executive function, and fractional anisotropy: a diffusion tensor MR imaging study. *AJNR Am J Neuroradiol*. 2007;28:226–235.
- Gunning-Dixon FM, Brickman AM, Cheng JC, Alexopoulos GS. Aging of cerebral white matter: a review of MRI findings. *Int J Geriatr Psychiatry*. 2009;24:109–117.
- Hansen ECA, Battaglia D, Spiegler A, Deco G, Jirsa VK. Functional connectivity dynamics: modeling the switching behavior of the resting state. *NeuroImage*. 2015;105:525–535.
- Hedden T, Schultz AP, Rieckmann A, Mormino EC, Johnson KA, Sperling RA, Buckner RL. Multiple brain markers are linked to age-related variation in cognition. *Cereb Cortex*. 2016;26:1388–1400.
- Heitmann S, Breakspear M. Putting the “dynamic” back into dynamic functional connectivity. *Netw Neurosci*. 2017;2(02):150–174.
- Hutchison RM, Womelsdorf T, Allen EA, Bandettini PA, Calhoun VD, Corbetta M, Della Penna S, Duyn JH, Glover GH, Gonzalez-Castillo J, et al. Dynamic functional connectivity: promise, issues, and interpretations. *NeuroImage*. 2013;80:360–378.
- Inano S, Takao H, Hayashi N, Abe O, Ohtomo K. Effects of age and gender on white matter integrity. *Am J Neuroradiol*. 2011;32:2103–2109.
- Jirsa V, Müller V. Cross-frequency coupling in real and virtual brain networks. *Front Comput Neurosci*. 2013;7:78.
- Jirsa VK, Proix T, Perdakis D, Woodman MM, Wang H, Bernard C, Bénar C, Chauvel P, Bartolomei F, Bartolomei F, et al. The virtual epileptic patient: individualized whole-brain models of epilepsy spread. *NeuroImage*. 2017;145:377–388.
- Jockwitz C, Caspers S, Lux S, Eickhoff SB, Jütten K, Lenzen S, Moebus S, Pundt N, Reid A, Hoffstaedter F, et al. Influence of age and cognitive performance on resting-state brain networks of older adults in a population-based cohort. *Cortex*. 2017;89:28–44.
- Johansen-Berg H, Rushworth MFS. Using diffusion imaging to study human connective anatomy. *Annu Rev Neurosci*. 2009;32:75–94.
- Kikuchi M, Wada Y, Koshino Y, Nanbu Y, Hashimoto T. Effect of normal aging upon interhemispheric EEG coherence: analysis during rest and photic stimulation. *ClinElectroencephalogr*. 2000;31:170–174.
- Knott VJ, Harr A. Aging, smoking and EEG coherence: a preliminary study. *Clin EEG Neurosci*. 1997;28:236–244.
- Kong X, Kong R, Orban C, Wang P, Zhang S, Anderson K, Holmes A, Murray JD, Deco G, van den Heuvel M, et al. Sensory-motor cortices shape functional connectivity dynamics in the human brain. *Nat Commun*. 2021;12(1):1–15.

- Kuramoto Y. *Chemical Oscillations, Waves, and Turbulence*. Vol. 19. Berlin, Heidelberg: Springer; 1984. Springer Series in Synergetics
- Lemaréchal JD, Jedynak M, Trebaul L, Boyer A, Tadel F, Bhattacharjee M, Deman P, Tuyisenge V, Ayoubian L, Hugues E, et al. A brain atlas of axonal and synaptic delays based on modelling of cortico-cortical evoked potentials. *Brain*. 2021;145(5):1653–1667.
- Li L, Lu B, Yan CG. Stability of dynamic functional architecture differs between brain networks and states. *NeuroImage*. 2020;216:116230.
- Lim S, Han CE, Uhlhaas PJ, Kaiser M. Preferential detachment during human brain development: age- and sex-specific structural connectivity in diffusion tensor imaging (DTI) data. *Cereb Cortex*. 2015;25:1477–1489.
- Logothetis NK, Pauls J, Augath M, Trinath T, Oeltermann A. Neurophysiological investigation of the basis of the fMRI signal. *Nature*. 2001;412:150–157.
- Lombardo D, Cassé-Perrot C, Ranjeva JP, Le Troter A, Guye M, Wirsich J, Payoux P, Bartrés-Faz D, Bordet R, Richardson JC, et al. Modular slowing of resting-state dynamic functional connectivity as a marker of cognitive dysfunction induced by sleep deprivation. *NeuroImage*. 2020;222:117155.
- Lövdén M, Bäckman L, Lindenberger U, Schaefer S, Schmiedek F. A theoretical framework for the study of adult cognitive plasticity. *Psychol Bull*. 2010;136:659.
- Lurie DJ, Kessler D, Bassett DS, Betzel RF, Breakspear M, Kheilholz S, Kucyi A, Liégeois R, Lindquist MA, McIntosh AR, et al. Questions and controversies in the study of time-varying functional connectivity in resting fMRI. *Netw Neurosci*. 2020;4:30–69.
- Mädler B, Drabycz SA, Kolind SH, Whittall KP, MacKay AL. Is diffusion anisotropy an accurate monitor of myelination? Correlation of multicomponent T2 relaxation and diffusion tensor anisotropy in human brain. *Magn Reson Imaging*. 2008;26:874–888.
- McIntosh AR, Jirsa VK. The hidden repertoire of brain dynamics and dysfunction. *Netw Neurosci*. 2019;3:994–1008.
- Musizza B, Stefanovska A, McClintock PVE, Palus M, Petrovic J, Ribaric S, Bajrovic FF. Interactions between cardiac, respiratory and EEG-delta oscillations in rats during anaesthesia. *J Physiol*. 2007;580:315–326.
- Nakagawa TT, Jirsa VK, Spiegler A, McIntosh AR, Deco G. Bottom up modeling of the connectome: linking structure and function in the resting brain and their changes in aging. *NeuroImage*. 2013;80:318–329.
- Newman MEJ, Girvan M. Finding and evaluating community structure in networks. *Phys Rev E*. 2004;69:026113.
- Olivares R, Montiel J, Aboitiz F. Species differences and similarities in the fine structure of the mammalian corpus callosum. *Brain Behav Evol*. 2001;57:98–105.
- Park DC, Reuter-Lorenz P. The adaptive brain: aging and neurocognitive scaffolding. *Annu Rev Psychol*. 2009;60:173.
- Pathak A, Roy D, Banerjee A. Whole-brain network models: from physics to bedside. *Front Comput Neurosci*. 2022a;16:1–12.
- Pathak A, Sharma V, Roy D, Banerjee A. Biophysical mechanism underlying compensatory preservation of neural synchrony over the adult lifespan. *Commun Biol*. 2022b;5:1–12.
- Perry A, Wen W, Lord A, Thalamuthu A, Roberts G, Mitchell PB, Sachdev PS, Breakspear M. The organisation of the elderly connectome. *NeuroImage*. 2015;114:414–426. 1502.05772.
- Peters A. The effects of normal aging on myelin and nerve fibers: a review. *J Neurocytol*. 2002;31:581–593.
- Peters R. Ageing and the brain. *Postgrad Med J*. 2006;82:84–88.
- Peters A, Sethares C. Aging and the myelinated fibers in prefrontal cortex and corpus callosum of the monkey. *J Comp Neurol*. 2002;442:277–291.
- Petkoski S, Jirsa VK. Transmission time delays organize the brain network synchronization. *Philos Trans Royal Soc A*. 2019;377:20180132.
- Petkoski S, Jirsa VK. Normalizing the brain connectome for communication through synchronization. *Netw Neurosci*. 2022;6:722–744.
- Petkoski S, Stefanovska A. Kuramoto model with time-varying parameters. *Phys Rev E Stat Nonlinear Soft Matter Phys*. 2012;86:1–7 1107.3867.
- Petkoski S, Spiegler A, Proix T, Aram P, Temprado JJJ, Jirsa VK. Heterogeneity of time delays determines synchronization of coupled oscillators. *Phys Rev E Stat Nonlinear Soft Matter Phys*. 2016;94:1–7 1606.08613.
- Petkoski S, Palva JM, Jirsa VK. Phase-lags in large scale brain synchronization: methodological considerations and in-silico analysis. *PLoS Comput Biol*. 2018;14:1–30.
- Pope M, Fukushima M, Betzel RF, Sporns O. Modular origins of high-amplitude co-fluctuations in fine-scale functional connectivity dynamics. *Proc Natl Acad Sci U S A*. 2021;118: 2021 May 16.444357.
- Puxeddu MG, Faskowitz J, Betzel RF, Petti M, Astolfi L, Sporns O. The modular organization of brain cortical connectivity across the human lifespan. *NeuroImage*. 2020;218:116974.
- Rabuffo G, Fousek J, Bernard C, Jirsa V. Neuronal cascades shape whole-brain functional dynamics at rest. *Biorxiv*. 2021:2020–2012.
- Reveley C, Seth AK, Pierpaoli C, Silva AC, Yu D, Saunders RC, Leopold DA, Frank QY. Superficial white matter fiber systems impede detection of long-range cortical connections in diffusion MR tractography. *Proc Natl Acad Sci*. 2015;112:E2820–E2828.
- Rodrigues FA, Peron TKDM, Ji P, Kurths J. The Kuramoto model in complex networks. *Phys Rep*. 2016;610:1–98 1511.07139.
- Rubinow M, Sporns O. Complex network measures of brain connectivity: uses and interpretations. *NeuroImage*. 2010;52:1059–1069.
- Sams E. Oligodendrocytes in the aging brain. *Neuronal Signal*. 2021;5:1–24.
- Sanz-Leon P, Knock SA, Spiegler A, Jirsa VK. Mathematical framework for large-scale brain network modeling in The Virtual Brain. *NeuroImage*. 2015;111:385–430.
- Sastry NC, Roy D, Banerjee A. Stability of sensorimotor network sculpts the dynamic repertoire of resting state over lifespan. *Cereb Cortex*. 2022:bhac133.
- Schirmer M, Rothmeier S, Jirsa VK, McIntosh AR, Ritter P. An automated pipeline for constructing personalized virtual brains from multimodal neuroimaging data. *NeuroImage*. 2015;117: 343–357.
- Schirmer M, McIntosh AR, Jirsa V, Deco G, Ritter P. Inferring multi-scale neural mechanisms with brain network modelling. *elife*. 2018;7:1–30.
- Schirmer M, Domide L, Perdikis D, Triebkorn P, Stefanovski L, Pai R, Prodan P, Valean B, Palmer J, Langford C, et al. Brain simulation as a cloud service: The Virtual Brain on EBRAINS. *NeuroImage*. 2022;251:118973.
- Sheppard LW, Hale AC, Petkoski S, McClintock PVE, Stefanovska A. Characterizing an ensemble of interacting oscillators: the mean-field variability index. *Phys Rev E Stat Nonlinear Soft Matter Phys*. 2013;87:1–11.
- Shine JM, Breakspear M, Bell PT, Ehgoetz Martens K, Shine R, Koyejo O, Sporns O, Poldrack RA. Human cognition involves the dynamic integration of neural activity and neuromodulatory systems. *Nat Neurosci*. 2019;22:289–296.
- Sip V, Petkoski S, Hashemi M, Jirsa V. Parameter inference on brain network models with unknown node dynamics and spatial heterogeneity. *bioRxiv*. 2021:1–25.
- Sleimen-Malkoun R, Temprado JJ, Hong SL. Aging induced loss of complexity and dedifferentiation: consequences for coordination

- dynamics within and between brain, muscular and behavioral levels. *Front Aging Neurosci.* 2014;6:1–1.
- Sorrentino P, Petkoski S, Sparaco M, Lopez ET, Rucco R, Signoriello E, Baseliace F, Bonavita S, Pirozzi M, Quarantelli M, et al. Whole-brain propagation delays in multiple sclerosis, a combined tractography - magnetoencephalography study. *J Neurosci.* 2022;42(47):8807–8816.
- Sporns O, Chialvo DR, Kaiser M, Hilgetag CC. Organization, development and function of complex brain networks. *Trends Cogn Sci.* 2004;8:418–425.
- Sporns O, Tononi G, Kötter R. The human connectome: a structural description of the human brain. *PLoS Comput Biol.* 2005;1:0245–0251.
- Stankovski T, Petkoski S, Smith AF, McClintock PVE, Stefanovska A, Raeder J, Smith AF, McClintock PVE, Stefanovska A. Alterations in the coupling functions between cortical and cardio-respiratory oscillations due to anaesthesia with propofol and sevoflurane. *Philos Trans R Soc A Math Phys Eng Sci.* 2016;374:20150186.
- Stankovski T, Pereira T, McClintock PVE, Stefanovska A. Coupling functions: universal insights into dynamical interaction mechanisms. *Rev Mod Phys.* 2017a;89:1–50 1706.01810.
- Stankovski T, Ticcinelli V, McClintock PVE, Stefanovska A. Neural cross-frequency coupling functions. *Front Syst Neurosci.* 2017b;11:33.
- Stefanovski L, Triebkorn P, Spiegler A, Diaz-Cortes MA, Solodkin A, Jirsa V, McIntosh AR, Ritter P. Linking molecular pathways and large-scale computational modeling to assess candidate disease mechanisms and pharmacodynamics in Alzheimer's disease. *Front Comput Neurosci.* 2019;13:54.
- Stumme J, Jockwitz C, Hoffstaedter F, Amunts K, Caspers S. Functional network reorganization in older adults: graph-theoretical analyses of age, cognition and sex. *NeuroImage.* 2020;214:116756.
- Suárez LE, Markello RD, Betzel RF, Misic B. Linking structure and function in macroscale brain networks. *Trends Cogn Sci.* 2020;24:302–315.
- Taylor NL, D'Souza A, Munn BR, Lv J, Zaborszky L, Müller EJ, Wainstein G, Calamante F, Shine JM. Structural connections between the noradrenergic and cholinergic system shape the dynamics of functional brain networks. *NeuroImage.* 2022;260:119455.
- Triebkorn, P, Zimmermann, J, Stefanovski, L., Roy, D, Solodkin, A., Jirsa, V, Deco, G., Breakspear, M., McIntosh, A.R., Ritter, P., 2020. Identifying optimal working points of individual virtual brains: a large-scale brain network modelling study. *BioRxiv.* doi.org/10.1101/2020.03.26.009795.
- Vincent JL, Patel GH, Fox MD, Snyder AZ, Baker JT, Van Essen DC, Zempel JM, Snyder LH, Corbetta M, Raichle ME. Intrinsic functional architecture in the anaesthetized monkey brain. *Nature.* 2007;447:83–86.
- Wang Z, Chen L, Négyessy L, Friedman R, Mishra A, Gore J, Roe A. The relationship of anatomical and functional connectivity to resting-state connectivity in primate somatosensory cortex. *Neuron.* 2013;78:1116–1126 NIHMS150003.
- Waxman SG. Determinants of conduction velocity in myelinated nerve fibers. *Muscle Nerve.* 1980;3:141–150.
- Wen W, Sachdev P. The topography of white matter hyperintensities on brain MRI in healthy 60- to 64-year-old individuals. *NeuroImage.* 2004;22:144–154.
- Xi MC, Liu RH, Engelhardt JK, Morales FR, Chase MH. Changes in the axonal conduction velocity of pyramidal tract neurons in the aged cat. *Neuroscience.* 1999;92:219–225.
- Xia Y, Chen Q, Shi L, Li M, Gong W, Chen H, Qiu J. Tracking the dynamic functional connectivity structure of the human brain across the adult lifespan. *Hum Brain Mapp.* 2019;40:717–728.
- Zalesky A, Fornito A, Cocchi L, Gollo LL, van den Heuvel MP, Breakspear M. Connectome sensitivity or specificity: which is more important? *NeuroImage.* 2016;142:407–420.
- Zhao T, Cao M, Niu H, Zuo XN, Evans A, He Y, Dong Q, Shu N. Age-related changes in the topological organization of the white matter structural connectome across the human lifespan. *Hum Brain Mapp.* 2015;36:3777–3792.
- Zimmermann J, Ritter P, Shen K, Rothmeier S, Schirner M, McIntosh AR. Structural architecture supports functional organization in the human aging brain at a regionwise and network level. *Hum Brain Mapp.* 2016;37:2645–2661.
- Zimmermann J, Griffiths JD, McIntosh AR. Unique mapping of structural and functional connectivity on cognition. *J Neurosci.* 2018;38:9658–9667.
- Zuo XN, He Y, Betzel RF, Colcombe S, Sporns O, Milham MP. Human connectomics across the life span. *Trends Cogn Sci.* 2016;21(1):32–45.